

Influence of Illumination Spectrum on Dissociation Kinetics_S of Iron-boron Pairs in Silicon

Oleg Olikh* Oleksandr Datsenko Serhiy Kondratenko

Prof. O. Olikh, Dr. O. Datsenko, Prof. S. Kondratenko

Taras Shevchenko National University of Kyiv, 64/13, Volodymyrska Street, 01601, Kyiv, Ukraine

Email Address: olegolikh@knu.ua

Keywords: *silicon, iron-boron pairs, light-induced dissociation, wavelength impact, dissociation rate*

Photo-dissociation kinetics of iron–boron (FeB) pairs in boron-doped Czochralski silicon was studied experimentally using different light sources. It was shown that the FeB dissociation rate depends not only on integrated light intensity and overall carrier generation rate, but also on spectral composition of illumination. The value of the material constant of dissociation K varies and has been determined to be within $(1.5 - 3.8) \times 10^{-15}$ s. The investigation has revealed an increase in the dissociation rate with increase in photon energy. The results indicate that recombination-enhanced defect reaction is the primary factor in the second stage of pair dissociation.

1 Introduction

Defects significantly impact semiconductor properties. Although when minimizing device dimensions to nanometers, focus some shifts from extended to point defects, physical properties still rely heavily on the presence and distribution of these irregularities. Hence, many strategies for enhancing semiconductor structures, including radiation and temperature treatments or certain fabrication conditions, strive to decrease the defect concentration or neutralize its effects [1, 2, 3]. For instance, in the case of photovoltaic devices, we must understand and optimize the carrier properties related to defects and impurities [1]. Such controlled alteration methods of the defect subsystem have been generalized under the term “defect engineering” and are extremely important from a practical standpoint.

Successful defect engineering hinges on an in-depth understanding of defect properties. Key factors are defect formation energy, transition energy levels, self-compensating effects, nonradiative recombination caused by defects, and the mechanism of reconstruction and diffusion [1]. Considering the extraordinary diversity of possible intrinsic and impurity defects, information on them is incomplete, even for silicon, which is the most studied semiconductor. Nevertheless, it must be noted that considerable data have been amassed on silicon, resulting in a solid understanding of certain defects [4].

For instance, iron impurity and iron-boron pairs are such defects that they are common, detrimental, and often unavoidable contaminants in photovoltaic silicon [3, 5]. Specifically, iron atoms are known to be at the interstitial sites, and Fe_i^+ are highly efficient recombination centers [6]. In p-type Si at room temperature, iron atoms are almost predominantly bound into complexes with dopants (B, Ga, Al, In). This defect demonstrates bistable behavior: the stable state is defined by the configuration in which Fe occupies the first nearest tetrahedral interstitial site closest to the substituent atom, whereas, in the metastable configuration, Fe is at the second T_d interstitial site [7]. The energy levels associated with iron and its complexes, as well as the respective carrier capture cross-sections, are well established [4, 8]. Among the acceptor-iron pairs, the complex FeB is the most thoroughly investigated, primarily due to the widespread use of Si:B in fabricating various devices, such as solar cells. However, it is worth mentioning that gallium is gaining more and more attention as an acceptor dopant whose incorporation, for instance, can help mitigate light and elevated temperature-induced degradation [9].

The dynamics of FeB pairs are also examined. It's established that FeB pairs can be dissociated through illumination, minority carrier injection, and thermal treatment at 200 °C [10]. In the context of illumination, the dissociation rate R_d is influenced by the overall carrier generation rate G [11, 10, 12, 13]:

$$R_d = K \left(\frac{G}{N_{\text{FeB}}} \right)^2, \quad (1)$$

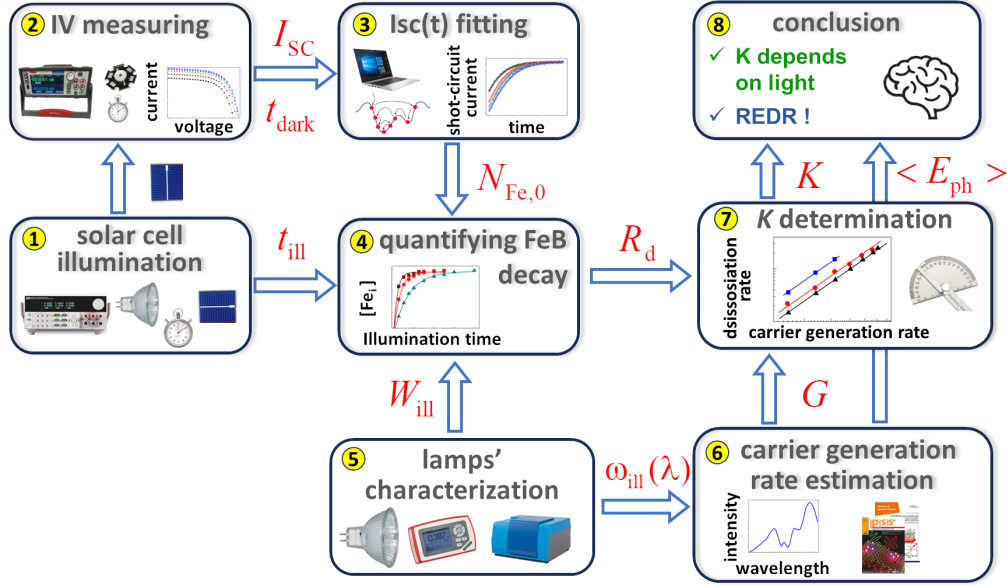


Figure 1: Investigation framework

where N_{FeB} is the pair concentration, K is the constant of the material. It is necessary for the illumination power to exceed 0.1 W cm^{-2} to achieve almost complete dissociation of the FeB pairs [14]. The dissociation process of FeB pairs by electron capture unfolds in two stages [15, 10]: the initial one involves the neutralization of Fe and the elimination of the Coulomb attraction between the pair components. The mechanism of the second stage is contentious; it may involve either the recharge of the iron ion or the recombination-enhanced defect reaction (REDR) triggered by electron-hole recombination.

It should be noted that despite the extensive data on the properties of iron-related defects in silicon, intensive research continues. In particular, efforts focus on analyzing the impact of high-intensive illumination [16] or dopant compensation [17], alongside clarifying the second-stage mechanism of dissociation [5] or reassessing recombination parameters [18].

This study aims to investigate the effect of the light spectrum on the dissociation kinetics of FeB pairs in silicon. While pair dissociation is typically carried out using a halogen lamp [11, 5] or a 904 nm laser [16, 10, 19], there is limited understanding of how the light source influences this process. By studying the impact of different illumination spectra on FeB dissociation, we aim to provide valuable insights for defect engineering and the efficient transformation of detrimental impurity iron atoms into a highly mobile interstitial state within the active region of a silicon device. Besides, such information, in our opinion, can help make the right choice between existing options for the second stage of pair decay.

In Figure 1, the main stages of the research are illustrated. First step was the determination of the dissociation rate of FeB pairs under illumination with different integral intensities. Three light sources from different manufacturers were used (box 1 on Figure 1, further details are described in Section 4). The kinetics of short-circuit current were used (boxes 2 and 3) to measure the number of interstitial iron atoms formed over fixed time under intense illumination (box 4). The result is presented in Subsection 2.1. Second step and Subsection 2.2 deal with estimating the carrier generation rate using spectra of sample illumination (box 5) and considering the effects of light reflection, absorption by free carriers, and effective absorption depths (box 6). The results showed that light-induced dissociation efficiency increases with decreasing photon wavelength — see Subsection 2.3 and box 7. Finally, we conclude this paper in Section 3 (box 8).

2 Results and Discussion

2.1 Dissociation rate determination

The equilibrium between free Fe_i and $\text{Fe}_i\text{B}_{\text{Si}}$ is known to be determined by the following equations [20, 5, 10]



where R_a is the association rate. As a result, the concentration of unpaired interstitial iron atoms N_{Fe_i} depending on illumination time t_{ill} during light-induced dissociation can be described as follows [11, 12, 21]

$$N_{\text{Fe}_i}(t_{\text{ill}}) = \left(N_{\text{Fe,eq}} - N_{\text{Fe,tot}} \frac{R_d}{R_d + R_a} \right) \exp[-(R_d + R_a)t_{\text{ill}}] + N_{\text{Fe,tot}} \frac{R_d}{R_d + R_a}, \quad (3)$$

where $N_{\text{Fe,tot}}$ is the total concentration of the impurity iron, $N_{\text{Fe,eq}}$ represents the concentration of unpaired interstitial iron atoms in the equilibrium state (in darkness, $N_{\text{Fe,eq}} = N_{\text{Fe}_i}(t_{\text{ill}} \leq 0)$). It is important to highlight that $N_{\text{Fe,eq}}$ is significantly influenced by temperature and the Fermi level location [20]. Specifically, in the case of p-type Si with a hole concentration $p = 1.36 \times 10^{15} \text{ cm}^{-3}$ (which corresponds to the structure under investigation), at a temperature of $T = 300 \text{ K}$, $N_{\text{Fe,eq}}$ is about 1 percent of $N_{\text{Fe,tot}}$, which is negligible for practical considerations. However, when the temperature rises to 340 K , the proportion of $N_{\text{Fe,eq}}$ increases to approximately 14.5%.

After stopping the illumination, only the process of association occurs, and the time dependence of Fe_i concentration can be expressed as follows [20, 22]:

$$N_{\text{Fe}_i}(t_{\text{dark}}) = (N_{\text{Fe},0} - N_{\text{Fe,eq}}) \times \exp(-R_a t_{\text{dark}}) + N_{\text{Fe,eq}}, \quad (4)$$

where t_{dark} is the time after stopping the strong illumination, $N_{\text{Fe},0}$ is the concentration of interstitial iron atoms formed after illumination, $N_{\text{Fe},0} = N_{\text{Fe}_i}(t_{\text{dark}} = 0) = N_{\text{Fe}_i}(t_{\text{ill}})$.

The study examined the dependence of $N_{\text{Fe},0}$ in silicon solar cells on illumination time t_{ill} using different integral illumination intensities W_{ill} ($200 - 750 \text{ mW}$) and light sources (three halogen lamps labeled as Orion, Osram, and GE and described in detail in Section 4). The experiments were conducted at a temperature of 340 K . The values of $N_{\text{Fe},0}$ were determined using a methodology [23, 21] based on fitting the kinetics of short-circuit current I_{SC} under low-intensity monochromatic illumination. Specifically, after strong illumination with a duration of t_{ill} , the current-voltage characteristic (I - V) of the solar cell was measured every 21 seconds over a time t_{dark} of about 3000 seconds.

Figure 2a shows some typical I - V curves. A gradual increase in both the short-circuit current and the open-circuit voltage is observed after the cessation of illumination. This indicates a decrease of the recombination activity of the defect subsystem, which is a result of the transition of interstitial iron to the bound state with the acceptor. Moreover, negligible changes in the I - V curves at the end of the measurement interval denote that the selected interval of 50 minutes is sufficient for complete association.

Figure 2b illustrates the dependencies $I_{SC}(t_{\text{dark}})$ after the illumination with different intensities. As shown previously [21], the magnitude of the change in I_{SC} after the dark recovery period inherently correlates with the concentration of Fe_i formed due to the light-induced dissociation of FeB pairs. The presented data evidence that the rise of W_{ill} leads to an increment in the dissociation efficiency. Meanwhile, the recovery time remains insensitive to the illumination parameters, which is expected, as the former is determined by R_a (see Equation (4)).

It should be noted that apart from $N_{\text{Fe},0}$, the fitting of short-circuit current [23, 21] allows for the estimation of the migration energy of Fe_i , E_m , and bulk lifetime τ_{other} of minority carriers, which is related to recombination channels other than Fe-related defects and intrinsic recombination. The obtained value $E_m = (0.650 \pm 0.005) \text{ eV}$ coincides with that known from Refs. [12, 24, 25]. This coincidence confirms that the investigated processes are indeed associated with rebuilding, as Equation (2) describes. In turn, the value of E_m allows for the estimation of the association rate [10, 12, 24]:

$$R_a^{-1} = 5.7 \times 10^5 \frac{\text{s}}{\text{K cm}^3} \times \frac{T}{p} \exp\left(\frac{E_m}{kT}\right). \quad (5)$$

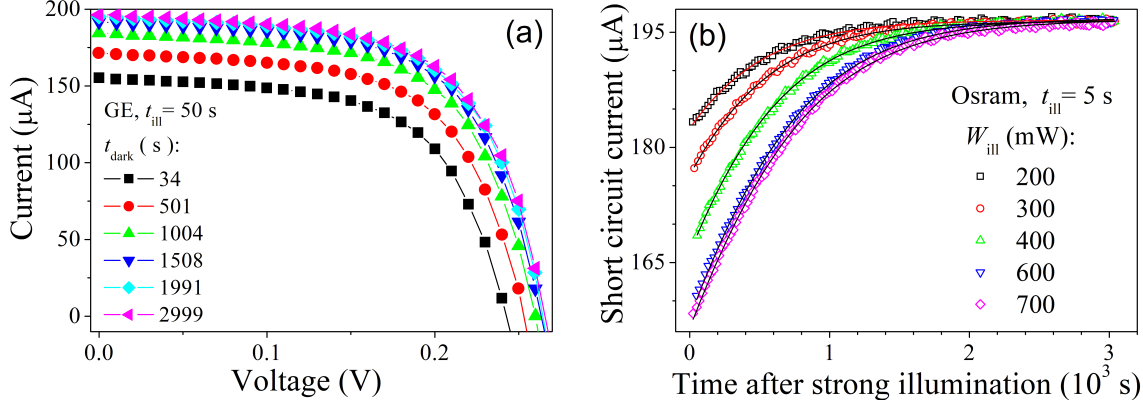


Figure 2: Typical I - V characteristics measured at $T = 340$ K under low-intense LED illumination at 940 nm after delays following the exposure for 50 s to intense (400 mW) light (GE lamp) (a) and short circuit current vs the delay time after the illumination for 5 s of Osram lamp with various intensities (b). The marks are the experimental data, and the lines on (b) are the fitting curves according to [23, 21].

Thus, in our case, $R_a = (1.68 \pm 0.03) \times 10^{-3} \text{ s}^{-1}$.

As for the value of τ_{other} , it was found to exceed significantly the lifetime associated with Shockley–Read–Hall (SRH) recombination on Fe-related defects. The last one is about 2.2 μs , whereas τ_{other} equals (20–300) μs for the samples of the same series. Notably, according Möller *et al.* [10], such a condition is essential for accurately determining the constant K , which is included in Equation (1).

The dependencies of the concentration of interstitial atoms on illumination time are shown in **Figure 3**. It is evident from the data that the pair dissociation rate is influenced significantly by the illumination intensity for all the used light sources. Nonetheless, the pair dissociation rate is not determined by the W_{ill} value only. As demonstrated in Figure 3d, pair dissociation under the GE source is the fastest. With Osram under otherwise identical conditions, the process is slower, while illumination with Orion proves to be the least effective in terms of altering the state of FeB pairs.

Considering Equation (3), the experimentally obtained dependencies $N_{\text{Fe},0}(t_{\text{ill}})$ were fitted using the function

$$N_{\text{Fe},0}(t_{\text{ill}}) = A \exp(-t_{\text{ill}}/\tau_{\text{dis}}) + B, \quad (6)$$

where τ_{dis} is the characteristic dissociation time, and B means the concentration of dissociated pairs at the saturation. The fitting parameters are collected in **Table 1**, including the coefficient of determination R^2 . The high values of R^2 (greater than 0.99) confirm the suitability of the chosen fitting formula. One can see from Equations (3) and (6) that the fitting parameters relate to defect characteristics:

$$\tau_{\text{dis}}^{-1} = R_a + R_d, \quad (7)$$

$$B = N_{\text{Fe,tot}} \frac{R_d}{R_d + R_a}. \quad (8)$$

The fitting parameters with considering the association rate of $1.68 \times 10^{-3} \text{ s}$ allow us to calculate the values of $N_{\text{Fe,tot}}$ and R_d , which are also collected in Table 1. As seen, the calculated values of the impurity iron atom concentration $N_{\text{Fe,tot}} = (8.7 \pm 0.1) \times 10^{12} \text{ cm}^{-3}$ are expectably independent of the light source and illumination intensity W_{ill} . This confirms the accuracy of the analysis. Contrariwise, the FeB dissociation rate may vary significantly with both the intensity value and the used light source.

According to Wijaranakula [20], the concentrations of interstitial iron atoms $N_{\text{Fe,eq}}$ and FeB pairs N_{FeB} before the illumination at the specified value of $N_{\text{Fe,tot}}$ and $T = 340$ K are $1.3 \times 10^{12} \text{ cm}^{-3}$ and $7.4 \times 10^{12} \text{ cm}^{-3}$, respectively. The values of $N_{\text{Fe,eq}}$ and N_{FeB} were used to estimate the minority carrier diffusion length L_n in the base of the used solar cell. It was assumed that the dominant recombination processes are SRH recombination at Fe_i and FeB and intrinsic recombination. The required value of electron mobility μ_n was taken from Klaassen [26], the capture cross sections and energy levels for Fe_i and FeB from Rougieux *et al.* [8], the parameters of band-to-band radiative recombination and Auger recombination from Niewelt *et al.* [27] and Black & Macdonald [28], respectively. The calculated value was

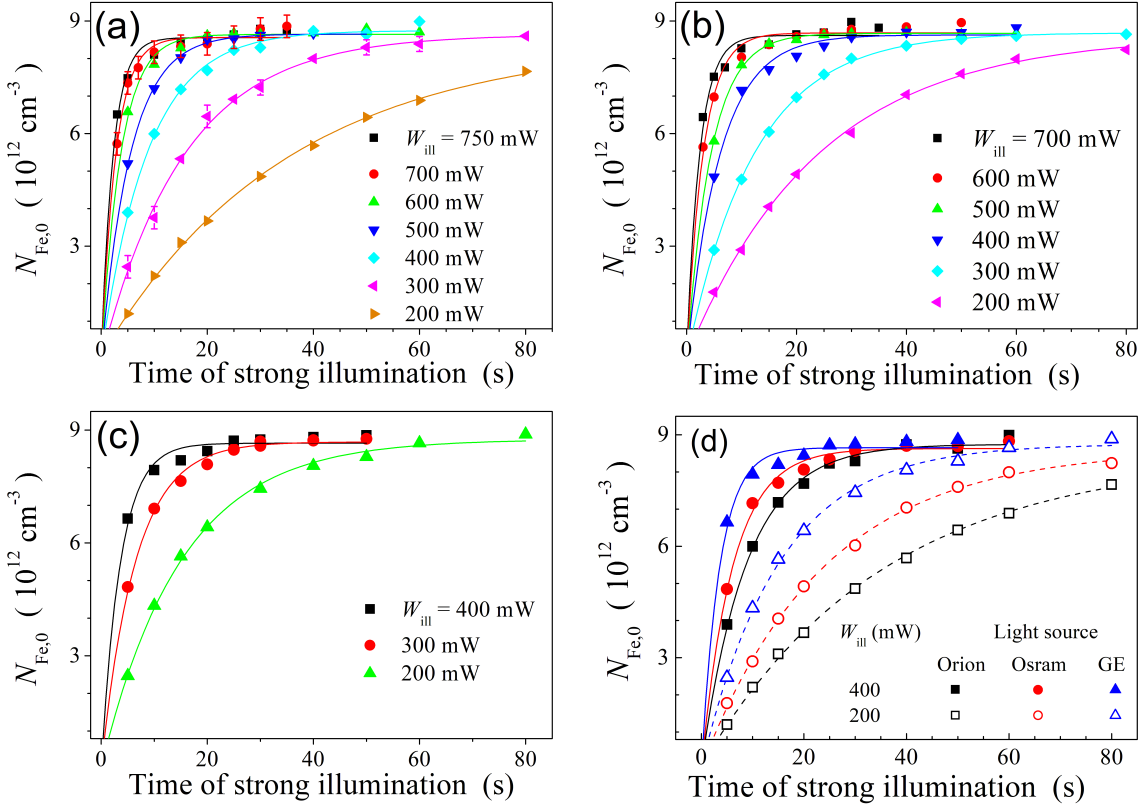


Figure 3: Rise of the dissociated FeB pair concentration under the illumination by sources Orion (a), Osram (b), GE (c) of different intensities ($T = 340$ K). Panel (d) compares the effect of different light sources. The marks are the experimental results, the lines are the fitting by Equation (6).

Table 1: Fitting parameters of experimental dependencies $N_{Fe,0}(t_{ill})$ using Equation (6) and defect parameters estimated using Equations (7-8).

W_{ill} [mW]	Light source	fitting parameters			defect parameters	
		τ_{dis} [s]	B [10^{12} cm 3]	R^2	R_d [10^{-3} s $^{-1}$]	$N_{Fe,tot}$ [10^{12} cm $^{-3}$]
750	Orion	2.2 ± 0.2	8.6 ± 0.1	0.993	450	8.6
	Osram	2.7 ± 0.2	8.7 ± 0.1	0.995	370	8.7
600	Orion	2.4 ± 0.2	8.6 ± 0.1	0.992	410	8.6
	Osram	3.7 ± 0.2	8.65 ± 0.06	0.998	270	8.7
500	Orion	3.0 ± 0.2	8.69 ± 0.08	0.995	330	8.7
	Osram	5.5 ± 0.2	8.65 ± 0.04	0.999	180	8.7
400	Orion	4.5 ± 0.1	8.7 ± 0.1	0.998	220	8.8
	Osram	8.8 ± 0.3	8.74 ± 0.06	0.998	110	8.8
300	GE	6.1 ± 0.2	8.63 ± 0.08	0.997	160	8.7
	Orion	15.7 ± 0.6	8.6 ± 0.1	0.998	280	8.7
	Osram	12.4 ± 0.1	8.69 ± 0.02	0.999	62	8.8
200	GE	6.5 ± 0.2	8.69 ± 0.05	0.998	79	8.8
	Orion	35 ± 3	8.5 ± 0.3	0.998	150	8.8
	Osram	24 ± 1	8.6 ± 0.1	0.999	40	8.9
	GE	15.1 ± 0.5	8.7 ± 0.1	0.999	65	8.8

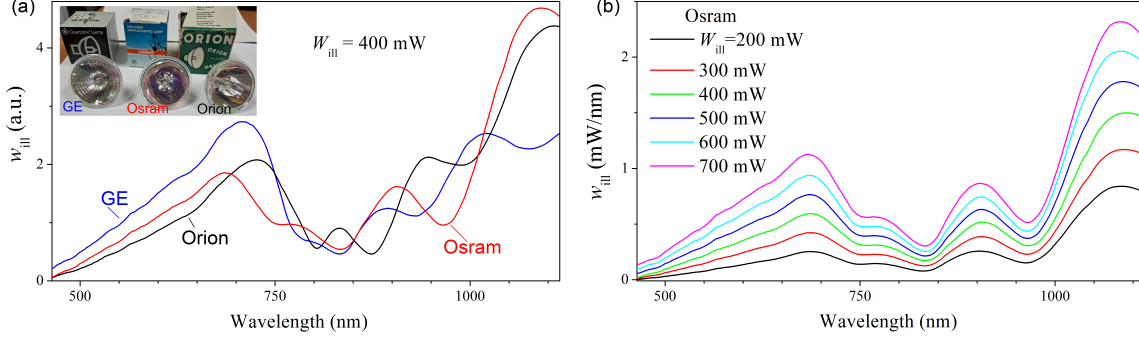


Figure 4: The spectra of sample illumination under different light sources with the same integral intensity $W_{\text{ill}} = 400 \text{ mW}$ (a) and Osram source at various W_{ill} values (b). The inset shows photos of light sources.

found to be $L_n = 80 \mu\text{m}$, which is very close to $86 \mu\text{m}$ obtained from the study of temperature dependencies of short-circuit current, see Supplementary materials.

2.2 Carrier generation rate estimation

The light-induced dissociation rate of FeB pairs is well known to be dependent on the carrier generation rate (see Eq. (1)). Our next aim was determining the values of G for various light sources. **Figure 4** shows the measured spectral intensity of illumination, w_{ill} , incident onto the sample surface. It is crucial to highlight that our focus is specifically on the light reaching the sample; hence, the brought spectra are distorted not only by the absorption of the lamp reflector and protective glass, but also by absorption in the fiber utilized to transmit the light flux to the solar cell. Other researchers have considered similar modifications of the illumination spectra [29]. Figure 4a displays discrepancies in the illumination spectra obtained from different light sources, attributed to variations in the operational temperatures of the halogen lamps and differences in reflectors (photos of the lamps are in the inset of Figure 4a). It is important to note that the upper limit of the spectra in Fig 4 (1120 nm) is limited by the silicon bandgap, which, according to Passler [30], corresponds to 1.11 eV at 340 K. Furthermore, Figure 4b demonstrates the change in the Osram spectrum with integral intensity increasing. Notably, in addition to the expected increase in the curve's area, a minor spectrum shift towards shorter wavelengths is observed. This behavior is typical for all used light sources.

The carrier generation rate was estimated as follows:

$$G = \int g(\lambda) d\lambda, \quad (9)$$

where the spectral density of carrier generation rate

$$g = \frac{w_{\text{ill}} \lambda}{hc} \frac{(1 - R) A_{\text{bb}}}{S d_{\text{eff}}}, \quad (10)$$

where $n_{\text{ph}} = \frac{w_{\text{ill}} \lambda}{hc}$ is the spectral photon flux, R is the reflectance, A_{bb} is the band-to-band fraction of the absorptance, S is the illuminated area of the sample, d_{eff} is the effective width of carrier generation. When calculating the value of R , we employed an approach [31], which considers the presence of antireflective and passivating layers on the front surface of the sample, as well as the effects of multiple reflections. The resulting spectral dependence of R is shown in Figure S3 of the Supplementary materials. The expression for the e-h pair generating fraction of the Lambertian absorptance in a solar cell can be written as [32]:

$$A_{\text{bb}}(\lambda) = \frac{\alpha_{\text{bb}}}{\alpha_{\text{bb}} + \alpha_{\text{fca}}} \frac{(1 - T_r)(1 + T_r)n_r^2}{n_r^2 - (n_r^2 - 1)T_r^2}, \quad (11)$$

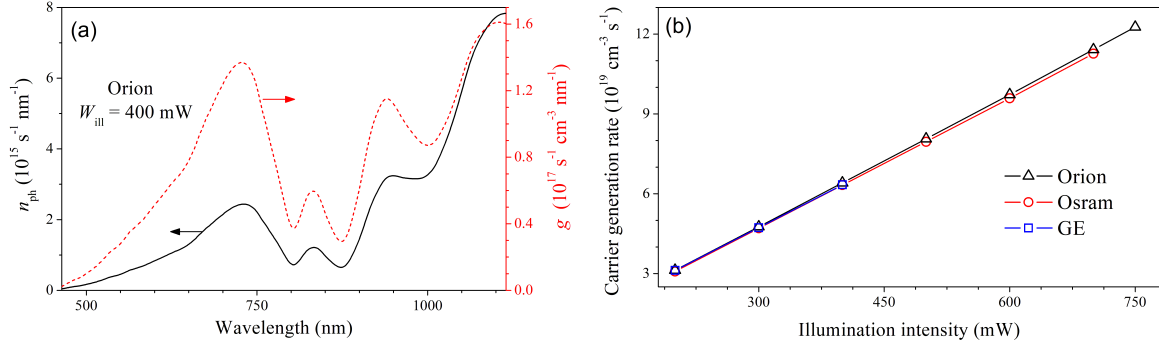


Figure 5: (a) Spectral densities of photon flux from Orion source at $W_{\text{ill}} = 400 \text{ mW}$ (left axis, solid line) and carrier generation rate (right axis, dashed line). (b) Dependencies of carrier generation rate on illumination intensity for different light sources.

with

$$\begin{aligned} T_r &= (1-x) \exp(-x) + x^2 E_1(x), \\ x &= (\alpha_{\text{bb}} + \alpha_{\text{fca}})d, \\ E_1(x) &= \int_x^\infty t^{-1} \exp(-t) dt, \end{aligned}$$

where α_{bb} is the band-to-band absorption coefficient; α_{fca} is the free carrier absorption coefficient; n_r is the refractive index; d is the width of the device.

In our calculations of A_{bb} by using Equation (11), we took α_{bb} and n_r from Green[33], α_{fca} from Baker-Finch *et al.* [34]. The spectral dependence of A_{bb} can be found in Supplementary materials (Figure S5). When determining the carrier generation volume, we applied the Bowden&Sinton approach [35] to thick silicon wafers, where the diffusion length or light absorption depth is significantly less than the sample thickness. In this case, the non-equilibrium carriers are concentrated near the illuminated surface, making using the arithmetic average of carrier concentration unsuitable. Therefore, the average values are calculated using carrier concentration as a weighting function, and effective generation width is determined as follows [35]:

$$d_{\text{eff}}(\lambda) = \frac{\left(\int_0^d \Delta n dx \right)^2}{\int_0^d \Delta n^2 dx}, \quad (12)$$

where Δn is the increase in minority carrier density due to illumination

$$\Delta n(x) = \frac{\alpha_{\text{bb}} n_{\text{ph}} L_n^2 q}{(\alpha_{\text{bb}}^2 L_n^2 - 1) k T \mu_n} \left[\exp\left(-\frac{x}{L_n}\right) - \exp(-\alpha_{\text{bb}} x) \right]. \quad (13)$$

In calculations, we used L_n value, determined in Subsection 2.1. Figure S4 (Supplementary materials) shows some dependencies of $d_{\text{eff}}(\lambda)$ for different L_n values.

The consideration of dependencies $R(\lambda)$, $A_{\text{bb}}(\lambda)$, and $d_{\text{eff}}(\lambda)$ modifies the spectral density of carrier generation rate compared to the spectrum of incident light, leading to an increased contribution to e-h pairs generated with shorter wavelengths, as illustrated in **Figure 5a**. In **Figure 5b**, variations of the total carrier generation rate G with increasing light intensity for different light sources are plotted. It is evident that differences exist between the light sources at the same W_{ill} , however, they are within 2 percent of the values; Orion source reveals the highest carrier generation rates.

Thus, the discrepancies noticed previously in the value of R_d (see Table 1) under identical illumination intensity levels cannot be attributed to variations in the carrier generation rate among different light sources, even when considering the quadratic dependency (1) of the dissociation rate on G . Hence, there must be another underlying cause for these differences.

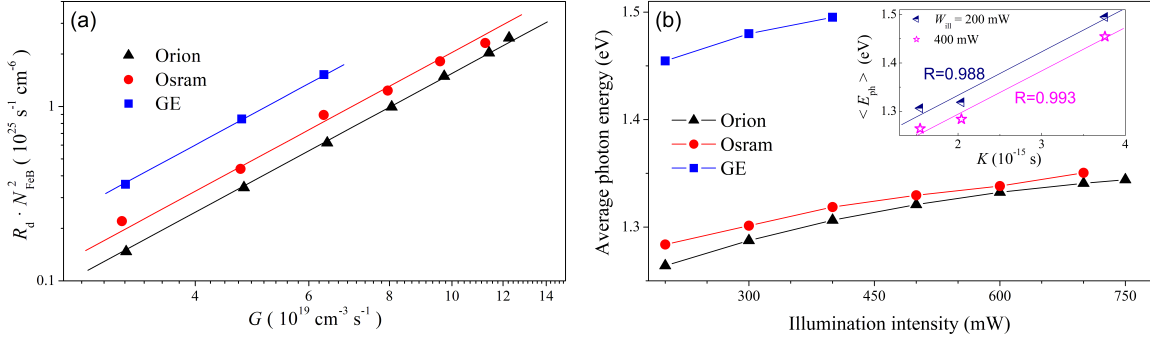


Figure 6: (a) FeB pair dissociation rate plotted as $(R_d \cdot N_{FeB}^2)$ versus the light-induced generation rate. The solid lines are the fitting with functions $\propto G^2$. (b) Dependencies of average photon energy on illumination intensity for different light sources. The inset shows pre-factor K vs average photon energy for the different light sources and illumination intensities. The lines are linear fitting curves. Coefficients of correlation are shown as well.

2.3 Effect of illumination spectrum on FeB pair decay

The dependencies $R_d(G)$ in the logarithmic scale are presented in **Figure 6a**. The lines are quadratic dependencies $\propto G^2$ fitting the experimental data using Equation (1). High correlation coefficients exceeding 0.998 validate the applicability of the quadratic dependence. It should be noted that Khelifati *et al.* [12] stipulated the change of R_d to $R_d(1 + \tau_{FeB}/\tau_{other})^2$ (τ_{FeB} is the lifetime associated with recombination on FeB pairs) on the left side of Equation (1). However, in our case $\tau_{other} \gg \tau_{FeB}$, as mentioned in Subsection 2.1, therefore, this additional multiplier may be neglected.

The prefactor K values determined from the fitting are $3.8 \times 10^{-15} \text{ s}$ for the GE light source, $2.0 \times 10^{-15} \text{ s}$ for the Osram, and $1.5 \times 10^{-15} \text{ s}$ for the Orion source. K is an important parameter related to the phenomenon of FeB pair dissociation caused by illumination [12], and the values obtained in this study are comparable to those ($4.2 \times 10^{-17} - 5 \times 10^{-15} \text{ s}$) presented in other studies [11, 10, 12]. It is worth noting that the variety of the constant K values for diverse samples in prior research was attributed to variations in defect composition and the presence of alternative recombination channels apart from iron-related defects [11, 10]. It should be noted that R_d is known to be temperature-dependent [36]. However, our values of K were obtained for the same structure under identical conditions, including temperature and integrated light intensity.

So, the obtained data indicate that, when analyzing light-induced dissociation of FeB pairs, it is necessary to consider not only the quantity of photo-generated charge carriers, but also the energies of the photons that lead to their appearance. For such an energy characterization of light sources, we used the average photon energy $\langle E_{ph} \rangle$:

$$\langle E_{ph} \rangle = \frac{\int \frac{hc}{\lambda} n_{ph}(\lambda) d\lambda}{\int n_{ph}(\lambda) d\lambda}. \quad (14)$$

The summary of the results concerning the $\langle E_{ph} \rangle$ values is shown in **Figure 6b**. In particular, it demonstrates a shift of the emission spectrum of light sources towards shorter waves with an increase in the W_{ill} value, as illustrated in Figure 4b. Comparing the data in Figure 3, 5b, 6a, 6b, and Table 1, one can conclude that the light-induced dissociation of FeB pairs becomes more pronounced with rising average photon energy. Specifically, the constant K and the dissociation rate R_d increase and, therefore, the illumination time necessary for a complete complex decay decreases. Hence, for the dissociation of FeB pairs, the energy expended during the thermalization of non-equilibrium carriers also holds significance. The obtained results offer some conclusions about the mechanism of FeB dissociation. As discussed in the literature and previously mentioned, two possible ways of the second decay stage are typically considered: recharge of the iron ion and REDR. The latter arises from strong electron-lattice coupling at the defect site and involves utilizing local vibrational energy to promote pair dissociation [10, 5, 14]. The observed correlation between dissociation rate and photon energy in this study confirms the REDR process. Specifically, as photon energy increases, the production of non-equilibrium phonons during thermalization also rises. Furthermore, the increase in R_d value found in the experiment means an active in-

vement of these quasi-particles in the dissociation of FeB pairs. Notably, recent research [5] focusing on a detailed analysis of the dissociation and association reactions of the iron–boron pairs similarly concluded the predominant role of REDR processes.

3 Conclusion

The effect of illumination spectra on the dissociation of FeB pairs in p–Si was investigated. We reported the results of an experimental study of FeB dissociation rate in a solar cell based on Cz–Si, which was carried out using different light sources and illumination intensities.

It was shown that the time required for the total dissociation of FeB pairs not only becomes shorter with increasing the illumination intensity, but also significantly depends on a light source. As a result, the determined value of material constant K varies within $(1.5 – 3.8) \times 10^{-15}$ s for the used light sources. The study of the illumination spectra allowed to conclude that the efficiency of FeB photo-dissociation increases with the photon energy. This, in turn, indicates that the REDR effect is the dominant factor during the second stage of light-induced dissociation of the FeB pairs. Furthermore, the obtained results could help to develop defect engineering procedures for effectively converting unintentional iron impurities in silicon into high-mobility states, which could significantly impact semiconductor technology.

4 Experimental Section

The $n^+‐p‐p^+$ -Si samples were used in the experiment. The structure was fabricated from a 380 μm thick p -type boron-doped Czochralski silicon (100) wafer with hole concentration $p = 1.36 \times 10^{15} \text{ cm}^{-3}$. The n^+ emitter with a sheet resistance of about $20 – 30 \Omega/\square$ and thickness of 0.7 μm was formed by phosphorus diffusion. The anti-recombination isotype barrier was created by using a p^+ layer ($10 – 20 \Omega/\square$, 0.6 μm) formed by boron diffusion. On the front surface, SiO_2 (40 nm) and Si_3N_4 (30 nm) films were formed as antireflective and passivating layers, respectively. The solid and grid Al contacts were formed by magnetron sputtering on the back and front surfaces, respectively.

A sufficiently high concentration of iron in the examined samples resulted from using impure chemicals during the chemical treatments in the technological process. This production flaw, which was subsequently corrected, allowed for the creation of model samples to study the effects associated with iron–boron pairs in silicon solar cells. Details regarding the iron contamination in the sample are described elsewhere [21]. The area of the samples used in the study was $1 \times 1 \text{ cm}^2$. The entire surface of the solar cell was illuminated during the experiments.

Three powerful halogen lamps from different manufacturers were used for sample illumination and were employed for the light-induced dissociation of FeB pairs:

- Orion Haltlichtspiegel 52240.0, 24 V, 200 W (labeled as “Orion” in the paper);
- Osram 64653 HLX ELC, 24 V, 250 W (Osram);
- General Electric 43537 H271, 20 V, 150 W (GE);

The light sources were powered by the DC Power Supply ITECH IT6332B, which allowed the current to be set through the lamp with an accuracy of 1 mA.

The illumination was transmitted from the sources to the sample via a fiber. The source emission at the fiber output underwent a calibration using an optical power and energy meter Thorlabs PM100D and a high-resolution sensor S401C, thereby enabling a direct assessment of the light flux incident on the sample. The illumination spectra at the fiber output were recorded using a spectrometer IKC-6 with a germanium photodiode with calibrated spectral sensitivity.

The current-voltage characteristics were measured using a Keithley 2450 source meter and low-intensity monochromatic light source (light-emitting diode SN-HPIR940nm-1W with light wavelength 940 nm and intensity of about 400 μW). The LED radiation intensity was stabilized by a W1209 thermostat and a power supply regulated by a circuit incorporating positive feedback and digital control.

The measurements were carried out at the temperature of 340 K. The sample temperature was driven by a thermoelectric cooler controlled by an STS-21 sensor and maintained constant by a PID algorithm embedded in the software that serves the experimental setup.

Supporting Information

Supporting Information is available from the Wiley Online Library or from the author.

Acknowledgements

The authors are grateful to Prof. Vitaliy Kostylyov for his help in calculating the reflectance of solar cells.

Conflict of Interest

The authors declare no conflict of interest.

Data Availability Statement

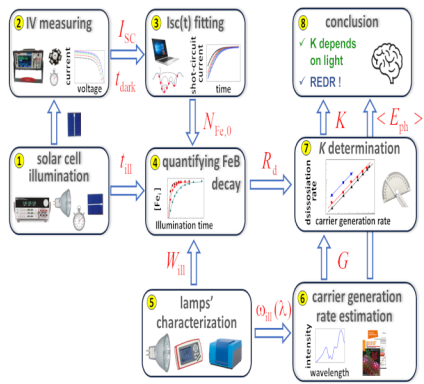
The data that support the findings of this study are available from the corresponding author upon reasonable request.

References

- [1] X. Cai, S.-H. Wei, *J. Appl. Phys.* **2023**, *134*, 22 220901.
- [2] J. Vobecky, *Phys. Status Solidi A* **2021**, *218*, 23 2100169.
- [3] J. Frascaroli, P. Monge Roffarello, I. Mica, *Phys. Status Solidi A* **2021**, *218*, 23 2100206.
- [4] M. K. Juhl, F. D. Heinz, G. Coletti, D. Macdonald, F. E. Rougier, F. Schindle, T. Niewelt, M. C. Schubert, In *2018 IEEE 7th World Conference on Photovoltaic Energy Conversion (WCPEC) (A Joint Conference of 45th IEEE PVSC, 28th PVSEC & 34th EU PVSEC)*. **2018** 0328–0332.
- [5] C. Sun, Y. Zhu, M. Juhl, W. Yang, F. Rougier, Z. Hameiri, D. Macdonald, *Phys. Status Solidi RRL* **2021**, *15*, 12 2000520.
- [6] E. Weber, *Appl. Phys. A* **1983**, *30*, 1 1.
- [7] H. Nakashima, T. Sadoh, T. Tsurushima, *Phys. Rev. B* **1994**, *49*, 24 16983.
- [8] F. E. Rougier, C. Sun, D. Macdonald, *Sol. Energy Mater. Sol. Cells* **2018**, *187* 263 .
- [9] L. Ning, L. Song, J. Zhang, *J. Alloys Compd.* **2022**, *912* 165120.
- [10] C. Möller, T. Bartel, F. Gibaja, K. Lauer, *J. Appl. Phys.* **2014**, *116*, 2 024503.
- [11] L. J. Geerligs, D. Macdonald, *Appl. Phys. Lett.* **2004**, *85*, 22 5227.
- [12] N. Khelifati, H. S. Laine, V. Vähänissi, H. Savin, F. Z. Bouamama, D. Bouhafs, *Phys Status Solidi A* **2019**, *216*, 17 1900253.
- [13] S. Herlufsen, D. Macdonald, K. Bothe, J. Schmidt, *physica status solidi (RRL) – Rapid Research Letters* **2012**, *6*, 1 1.
- [14] D. H. Macdonald, L. J. Geerligs, A. Azzizi, *J. Appl. Phys.* **2004**, *95*, 3 1021.
- [15] L. Kimerling, J. Benton, *Physica B+C* **1983**, *116*, 1 297.
- [16] X. Zhu, D. Yang, X. Yu, J. He, Y. Wu, J. Vanhellemont, D. Que, *AIP Adv.* **2013**, *3*, 8 082124.
- [17] X. Zhu, X. Yu, P. Chen, Y. Liu, J. Vanhellemont, D. Yang, *Int. J. Photoenergy* **2015**, *2015* 154574.
- [18] T. T. Le, Z. Zhou, A. Chen, Z. Yang, F. Rougier, D. Macdonald, A. Liu, *J. Appl. Phys.* **2024**, *135*, 13 133107.

- [19] K. Lauer, C. Möller, D. Debbih, M. Auge, D. Schulze, In *Gettering and Defect Engineering in Semiconductor Technology XVI*, volume 242 of *Solid State Phenomena*. Trans Tech Publications Ltd, **2016** 230–235.
- [20] W. Wijaranakula, *J. Electrochem. Soc.* **1993**, *140*, 1 275.
- [21] O. Olikh, V. Kostylyov, V. Vlasiuk, R. Korkishko, Y. Olikh, R. Chupryna, *J. Appl. Phys.* **2021**, *130*, 23 235703.
- [22] J. D. Murphy, K. Bothe, M. Olmo, V. V. Voronkov, R. J. Falster, *J. Appl. Phys.* **2011**, *110*, 5 053713.
- [23] O. Olikh, V. Kostylyov, V. Vlasiuk, R. Korkishko, R. Chupryna, *J. Mater. Sci.: Mater. Electron.* **2022**, *33*, 16 13133.
- [24] J. Tan, D. Macdonald, F. Rougier, A. Cuevas, *Semicond Sci. Technol.* **2011**, *26*, 5 055019.
- [25] D. Macdonald, A. Cuevas, L. J. Geerligs, *Appl. Phys. Lett.* **2008**, *92*, 20 202119.
- [26] D. Klaassen, *Solid-State Electron.* **1992**, *35*, 7 953.
- [27] T. Niewelt, B. Steinhauser, A. Richter, B. Veith-Wolf, A. Fell, B. Hammann, N. Grant, L. Black, J. Tan, A. Youssef, J. Murphy, J. Schmidt, M. Schubert, S. Glunz, *Sol. Energ. Mat. Sol.* **2022**, *235* 111467.
- [28] L. E. Black, D. H. Macdonald, *Sol. Energ. Mat. Sol.* **2022**, *234* 111428.
- [29] M. Libra, V. Poulek, P. Kourim, *Research in Agricultural Engineering* **2017**, *63*, 1 10.
- [30] R. Pässler, *Phys. Rev. B* **2002**, *66* 085201.
- [31] N. Klyui, V. Kostylyov, A. Rozhin, V. Gorbulik, V. Litovchenko, M. Voronkin, N. Zaika, *Opto-Electr. Rev.* **2000**, *8*, 4 402.
- [32] S. Schäfer, R. Brendel, *IEEE J. Photovolt.* **2018**, *8*, 4 1156.
- [33] M. A. Green, *Prog. Photovoltaics Res. Appl.* **2022**, *30*, 2 164.
- [34] S. C. Baker-Finch, K. R. McIntosh, D. Yan, K. C. Fong, T. C. Kho, *J. Appl. Phys.* **2014**, *116*, 6 063106.
- [35] S. Bowden, R. A. Sinton, *J. Appl. Phys.* **2007**, *102*, 12 124501.
- [36] J. Lagowski, P. Edelman, A. M. Kontkiewicz, O. Milic, W. Henley, M. Dexter, L. Jastrzebski, A. M. Hoff, *Appl. Phys. Lett.* **1993**, *63*, 22 3043.

Table of Contents



The results of an study on the kinetic of dissociation of FeB pairs in Cz-Si:B using different light sources are reported. Dissociation rate was shown to depend not only on intensity but also on spectral composition of illumination. The investigation has revealed increase in the dissociation efficiency with a decrease in wavelength and dominant role of the recombination-enhanced defect reaction